Strong negative thermal expansion in a low-cost and facile oxide of $Cu_2P_2O_7$

Naike Shi,[1] Andrea Sanson,[2] Qilong Gao,[3] Qiang Sun,[3] Yang Ren,[4] Qingzhen Huang,[5] Danilo Oliveira de Souza[6], Xianran Xing[1] and Jun Chen[*,1]

1 Beijing Advanced Innovation Center for Materials Genome Engineering, and Department of Physical Chemistry, University of Science and Technology Beijing, Beijing 100083, China.

2 Department of Physics and Astronomy, University of Padova, Padova I-35131, Italy

3 School of Physics and Engineering, Zhengzhou University, Zhengzhou 450001, China

4 X-ray Science Division, Argonne National Laboratory, Argonne, Illinois 60439, USA

5 NIST Center for Neutron Research, National Institute of Standards and Technology, Gaithersburg, Maryland 20899-6102, United States

6 Elettra Sincrotrone Trieste, 34149 Basovizza, Italy

ABSTRACT: Negative thermal expansion (NTE) behaviors have been observed in various types of compounds. The achievement in the merits of promising low-cost and facile NTE oxides remains challenging. In the present work, a simple and low-cost $Cu_2P_2O_7$ has been found to exhibit the strongest NTE among the oxides (αv ~ -27.69×10-6 K-1, 5K ~ 375K). The complex NTE mechanism has been investigated by combined methods of high resolution synchrotron X-ray diffraction, neutron powder diffraction, X-ray pair distribution function, extended X-ray absorption fine structure spectroscopy and density functional theory calculations. Interesting, the direct experimental evidence reveals that the coupling twist and rotation of PO_4 and CuO_5 polyhedra are the inherent factors for the NTE nature of $Cu_2P_2O_7$, which are triggered by the transvers vibrations of oxygen atoms. The present new NTE material of $Cu_2P_2O_7$ also has been verified the value for the practical application.

Introduction

Negative thermal expansion (NTE), which shows volume contraction upon heating, is a counterintuitive thermophysical behavior. Considerable interest has been attracted due to its both basic scientific value and practical application demands. It is known that most materials show positive thermal expansion (PTE) aroused by increasing anharmonic vibrational amplitudes of the constituent atoms. The mismatch in coefficient of thermal expansion (CTE) for device or engineering applications can be solved by the combination of PTE and NTE materials. Since 1996, the studies on NTE oxide of ZrW_2O_8 has provoked the rapid progress in the development of NTE[1]. The mode of rigid unit modes (RUMs) was used by Pryde, A. K. et al to elucidate NTE property in ZrW_2O_8[2], in which the coupling rotation of rigid polyhedra driven by low-frequency phonon are supposed for the reason of NTE. Except for the low-frequency phonon driven NTE in open framework structures, diverse attributions of electron roles can give rise to the NTE behavior, like magneto volume effect in antiperovskite manganese nitrides Mn_3AN (A= Zn, Ga, etc.) and $NaZn_{13}$-type compounds[3-5], ferroelectric phase transitions in perovskite (ABO_3) group[6,7], size effect in nanoparticles[8], and valence transition in some oxides[9-11]. Note that those electron-driven NTE behaviors can present strong NTE magnitude but a relatively narrow temperature range[12]. As a comparison, the low-frequency phonon driven NTE materials have a merit of wider NTE temperature range but relatively small NTE magnitude, such as oxides[13-15], fluorides[16,17], cyanides[18,19], Prussian blue analogues (PBAs)[20-23], and metal–organic frameworks (MOFs)[24,25]. All the low-energy phonon driven NTE materials own a common character of framework structure which is in corner shared tetrahedral or octahedral units through M-O-M, M-F-M or M-C≡N-M bridges. Generally, flexible framework structures with soft chemical bonds can contribute to a stronger NTE behavior, thus the NTE in oxides or fluorides generally smaller than that in PBAs or MOFs. As for applications, the oxides are more promising due to the thermal stable merit. Therefore, it is intriguing to explore facial oxides with strong NTE.

Various NTE oxides has been found besides ZrW2O8, especially $M_2V_2O_7$ formula attracted many attentions recent years since its facial synthesis and easy CTE tuned[26-27]. Herein, we have found a new NTE material $Cu_2P_2O_7$, which possesses similar structure with β-$Cu_2V_2O_7$ but shows superior NTE performance. $Cu_2P_2O_7$ exhibits not only the strongest NTE (α_v = -27.69 × 10^{-6} K^{-1}) in the oxides, but also the promising application merits of low cost

and facial fabrication. The NTE temperature range is from 13K to 373K which covers the room temperature. $Cu_2P_2O_7$ is in α-phase (space group *C*2/*c*) at room temperature, and undergoes a phase transition from α-phase to β-phase (space group *C*2/*m*) around 350 K. The crystal structure and NTE mechanism have been conducted by joined temperature dependence of high-resolution synchrotron X-ray diffraction (SXRD), neutron powder diffraction (NPD), pair distribution function (PDF), extended X-ray absorption fine structure (EXAFS), and density functional theory calculations (DFT). The NTE of $Cu_2P_2O_7$ is caused by the transverse vibrations of O atoms, which drives the twist and rotation of CuO_5 and PO_4 polyhedra. $Cu_2P_2O_7$ can be a unique promising NTE material for applications, which benefits from good comprehensive performances.

Result and discussion

The crystal structure and the thermal expansion property of $Cu_2P_2O_7$ have been determined by temperature dependence of both NPD (5~500K) and high-resolution SXRD (100K~775K). Below 350K, the crystal structure refinement of $Cu_2P_2O_7$ can be performed well with the α-phase model (*C*2/*c* space group). In accordance with previous report[28], the low-temperature α-phase is comprised of consecutive layers of CuO_5 zigzag columns and pairwise PO_4 tetrahedra (Figure 1). Distorted CuO_5 polyhedra are linked via shared O2-O2 and O3-O3 edges. Adjusted layers of CuO_5 polyhedra are linked with $[P_2O_7]$ groups, which consist of two $[PO4]^{3-}$ tetrahedra sharing one corner with the bridging O1 atom. With increasing temperature, $Cu_2P_2O_7$ goes through a phase transition gradually to a high temperature β-phase (*C*2/*m*). The O1 atoms of the β-phase become disorder in two equivalent positions, while they are antiparallel ordered in the low temperature α-phase. As a result, the *c* lattice parameter is doubled in the α-phase. The temperature evolution SXRD spectra from α-phase to β-phase are represented in Figure S1. Higher crystal symmetry accounts to less diffraction peaks in the β phase.

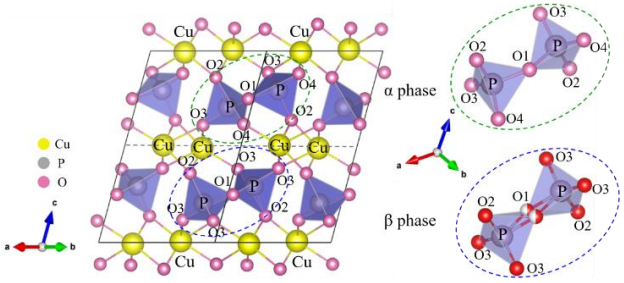

Fascinatingly, $Cu_2P_2O_7$ shows an abnormal NTE in the α-phase (5K – 375K), which has been verified by both high resolution SXRD and NPD measurements (Figure 2, Figure S2 and Figure S3). In the α-phase, both lattice parameters of *a* and *c* decrease rapidly, while *b* slightly increases with increasing temperature. However, all axes show positive thermal expansion once temperature reaches in the β-phase (above 375K). In the NTE temperature range, the CTE for lattice parameters are $\alpha_a = -30.11 \times 10^{-6}$ K^{-1}, $\alpha_b = 3.45 \times 10^{-6}$ K^{-1} and $\alpha_c = -10.75 \times 10^{-6}$ K^{-1}. Due to the strong shrinkage in the lattice parameters of *a* and *c*, strong negative thermal expansion happens in the unit cell volume (α_v ~ -27.69×10^{-6} K^{-1} ,5K - 375K). It is very interesting to find that the NTE effect in the present $Cu_2P_2O_7$ is the strongest among all the oxides (Figure 3). For example, it is slightly larger than the classical NTE material of ZrW_2O_8 (α_v ~ -26.1×10^{-6} K^{-1}, 0.3 - 693K)[29], and superior than other framework NTE oxides, such as ZrV_2O_7 (α_v ~ -21×10^{-6} K^{-1}, 473 - 873K)[30], $TaVO_5$ (α_v ~ -8.9×10^{-6} K^{-1}, 293-873K)[31], α-$Cu_2V_2O_7$ (α_v ~ -10.2×10^{-6} K^{-1}, 200-500K), β-$Cu_{1.8}Zn_{0.2}V_2O_7$ (α_v ~ -9.1×10^{-6} K^{-1},300-800K)[26], and $Sc_2(WO_4)_3$ (α_v ~ -6.5×10^{-6} K^{-1}, 50 - 450K)[32]. Intriguingly, the magnitude of such a strong NTE behavior in $Cu_2P_2O_7$ is about as large as the PTE effect in those conventional materials[12], which gives good chances to its practical application of counteracting thermal expansion.

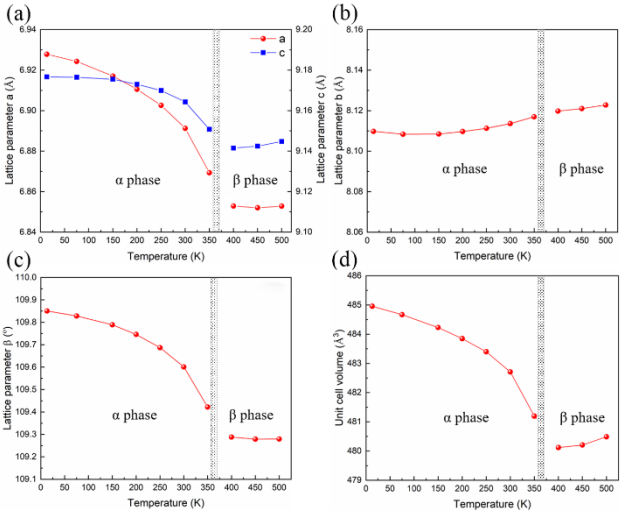

Figure 2. Temperature evolution of lattice parameters of $Cu_2P_2O_7$ derived from NPD. The shadow area refers to the phase transition. Note that the values of lattice parameter *c* and unit cell volume of the β-phase is doubled in order for the comparison with that of the α-phase.

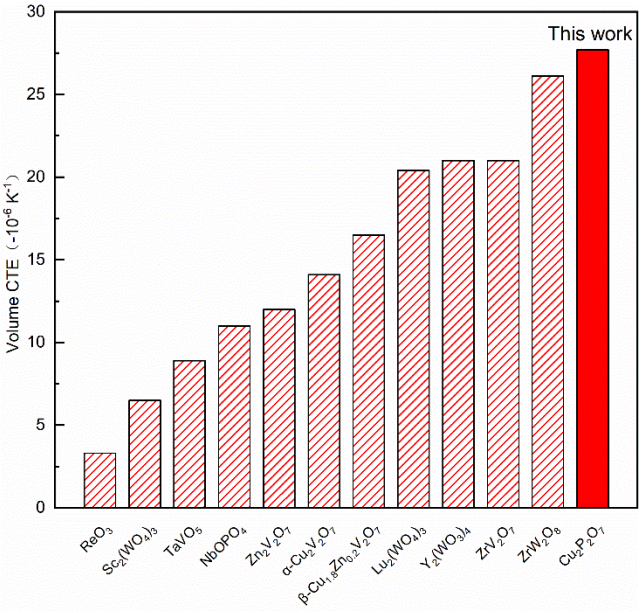

Figure 3. Comparison of NTE properties in the framework oxides [26, 29-38].

Due to the facts that the present $Cu_2P_2O_7$ compound consists of many light atoms of P and O, and especially O atoms often play important roles in NTE, temperature dependence of neutron diffraction has been performed to get accurate structure evolution information for understanding the NTE mechanism. The NPD refinement results show that in the α-$Cu_2P_2O_7$, every Cu atom is coordinated with two O2 and O3 atoms, as well as one O4 atom. Each P atom possesses four different oxygen ligands (Figure 4a). In the β phase, O4 evolves to the same position with O3, and O1 occupies two equivalent positions disorderly. To tell different bonds in the CuO_5 pentahedra, suffix "(long)" and "(short)" are added to refer to the longer and shorter bond lengths for same atoms. From temperature dependent NPD results, it was found that the overall changes of the temperature dependence of bond lengths and angles in CuO_5 and PO_4 polyhedra are small in the NTE temperature range, except Cu-O3(long) expands apparently (Figure 4b, and Figure S4). Especially, the PO_4 polyhedra are almost rigid, which indicates that the variation in polyhedra is not the cause of NTE in this oxide.

More experimental evidence can verify the rigidity in the PO_4 and CuO_5 polyhedra. From the temperature dependent PDF results (Figure 4c), the peak of P-O bonds shows little change with increasing temperature, which confirms the rigid body of PO_4 polyhedra. The Cu-O peak broadens to some extent. The thermal expansions of Cu-O bonds can be also demonstrated by EXAFS results (Figure 4d-f). During the fitting simulation for EXAFS, there are too much scattering paths below the first two Fourier transform (FT) peaks, hence the five Cu-O distances have been grouped in three Cu-O distances as shown in Table S1. This strategy is reasonable and useful. Because in the β phase, there are only two Cu-O distances below the first peak. Usually, the "true" bond lengths measured by EXAFS shows larger PTE than the "apparent" bond lengths measured by Bragg diffraction[39]. However, the Cu-O3(long) distance strongly expands and so its contribution exits from the first FT peak. This is the reason why the Cu-O3(long) bond expansion measured by EXAFS is lower than that by NPD. Above analyses reveal the PO_4 polyhedra are rigid, and the thermal expansion in CuO_5 polyhedra is on account of the Cu-O3(long).

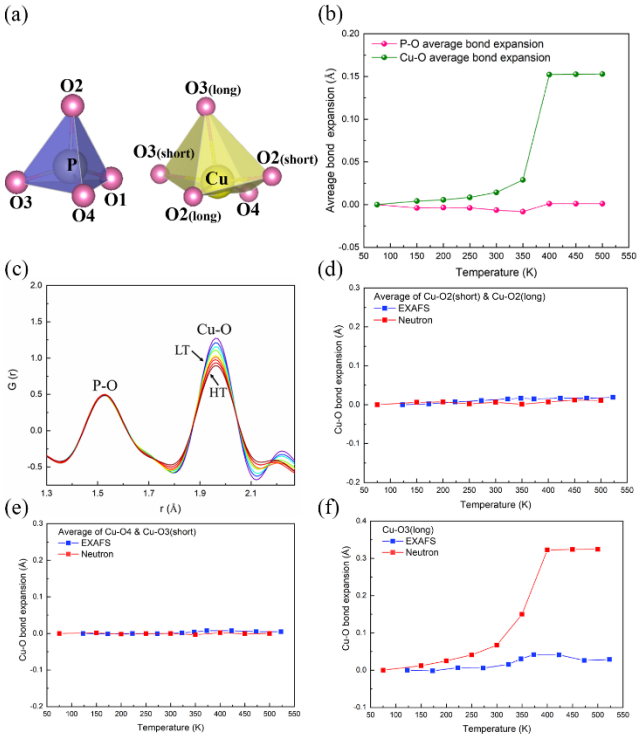

Figure 4. (a)Illustrations of PO_4 (the left one) and CuO_5 (the right one) polyhedra in $Cu_2P_2O_7$. (b) Variations of average Cu-O and P-O bonds determined from NPD. (c)Temperature dependent PDF spectra of the first P-O peak and Cu-O peak from 148K to 523K (the blue line is at low temperature, and the red line is at high temperature). (d)-(f) Comparison of thermal expansion in bond lengths in CuO_5 polyhedra determined from EXAFS and NPD.

What leads to the NTE behavior in the α-$Cu_2P_2O_7$? As shown in Figure 5a, the nonbonded distances and angles are analyzed as a function of temperature. Interestingly, the nonbonded Cu···Cu and Cu···P distances show a significant decrease, which agrees well with the volume contraction in $Cu_2P_2O_7$ (Figure 5, and Figure S6). In the NTE temperature range, the bond angle (θ) of Cu-O4-P reduces from 145.46° to 136.07°, which correspondingly shortens the nonbondend Cu···P distance. The bending of Cu-O4-P angle also drags the central Cu atoms closer, revealed by the reduced distance of the nonbonded Cu···Cu with increasing temperature. The decline of nonbonded Cu···P and Cu···Cu distances result the contract in the *a* axis. When the thermal expansion of $Cu_2P_2O_7$ turns to positive, the above parameters get nearly invariable or increase slightly. Meanwhile, the distance between $[P_2O_7]^{4-}$ layers also decreases, resulting in the shrinkage in the c axis. Consequently, the NTE in $Cu_2P_2O_7$ could result from the coupling twist and rotation of neighbor rigid polyhedra. The NTE nature of $Cu_2P_2O_7$ is entangled with RUMs, which is similar to some framework structure NTE materials, such as ZrW_2O_8[29], ScF_3[16], and Prussian blue analogues[23].

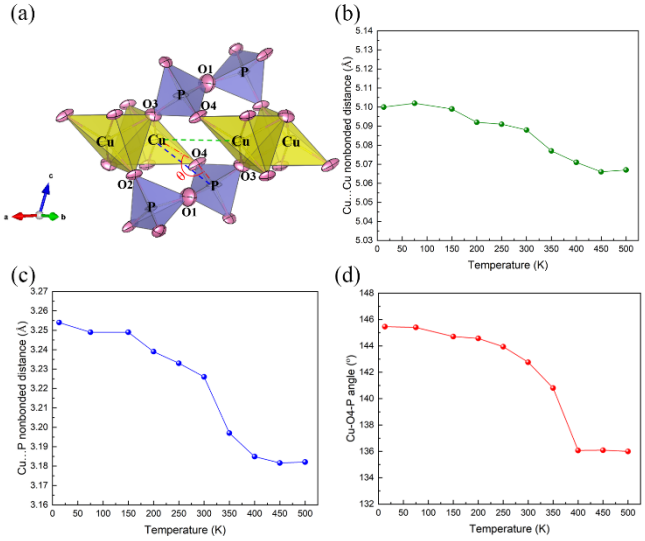

Figure 5. (a) Structure illustration of α-$Cu_2P_2O_7$. The green and blue dotted lines refer to the nonbonded Cu⋯Cu and Cu ⋯P distances, respectively. The θ refers to the Cu-O4-P angle. (b) The nonbonded of Cu⋯Cu distance, (c) the Cu⋯P nonbonded distance, and (d) the Cu-O4-P angle as function of temperature derived from NPD.

To reveal the inherent factors that trigger the rotation of rigid bodies leading to NTE, more information about vibrational motion has been extracted from the temperature dependent NPD and EXAFS data. Atomic displacement parameters (ADPs) are obtained from the NPD refinement (Figure 6a). It is interesting to find that strong anisotropic APDs can be observed in O1 and O4, as Figure 5a illustrated. Large U22 of O1 and U11 of O4 increase more rapidly than other ADPs in the NTE temperature range, which are related to transvers displacements of O1 and O4. After the temperature exceeds the phase transition point, this trend changes apparently. The U22 of O1 decreases suddenly, and the U11 of O4 maintains nearly invariant. The transverse thermal vibration behavior of oxygen can be directly determined from the atomic mean-square relative displacements (MSRDs) by Cu K-edge EXAFS (Figure 6b-d). The anisotropy displacements of the Cu-O bonds exhibit large transverse vibrations. The perpendicular $MSRD_{\perp}$ for all Cu-O bonds is much enhanced in the NTE temperature range, while declines in the PTE. The parallel $MSRD_{||}$ maintains slightly increase, responding to the thermal expansion of true Cu-O bonds (Figure 6b). In particularly, $MSRD_{\perp}$ for the Cu-O bonds is much larger than $MSRD_{||}$, quantitated by the large value of $\gamma = MSRD_{\perp} / MSRD_{||}$ (Figure 6d). It indicates the large transverse Cu-O vibrations. Over 350K, γ for all Cu-O bonds falls off apparently. It needs to note that the EXAFS of P atoms cannot be determined. The behavior of transverse vibrations of O1 has been revealed by ADPs of NPD (Figure 6a). All experimental evidences reveal that the large dynamically transverse motion of oxygen atoms, especially that of O1 and O4, is inherent factor deriving the coupling twist and rotation of rigid CuO_5 and PO_4 polyhedra in the NTE $Cu_2P_2O_7$.

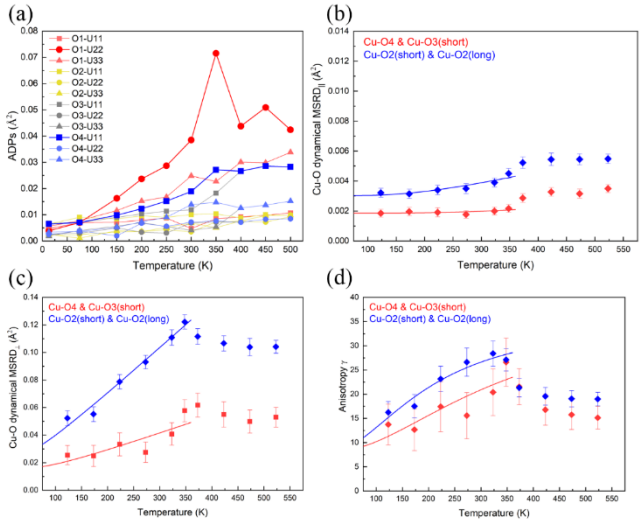

Figure 6. (a) ADPs of all oxygen atoms from NPD, (b) perpendicular ($MSRD_{\perp}$), (c) parallel ($MSRD_{||}$) to the related Cu-O bonds direction from EXAFS, and (d) anisotropy γ of the relative thermal vibrations of Cu-O atomic pairs of $Cu_2P_2O_7$ as function of temperature. The solid lines in (b) - (d) indicate the corresponding best-fitting Einstein models used in the range 125-350 K[40].

The lattice dynamics of oxygen atoms also have been verified by density functional theory (DFT) calculations. The crystal structure is optimized by the constrain of the experimental structure. As shown in Figure 7, low-frequency mode at ~68 cm^{-1} of α-phase and ~43 cm^{-1} of β-phase are illustrated. In the α-phase, transverse vibration of O1 atoms is strong and other oxygen atoms also show obvious transverse vibrations. However, the vibration of other oxygen atoms in the β-phase are restricted severely, although relatively large transverse vibrations still exist in the O1 atoms. In brief, the decay of transverse vibrations of oxygen atoms makes the whole structure more stiff leading to the disappearance of NTE, which is consisted with the above experimental results.

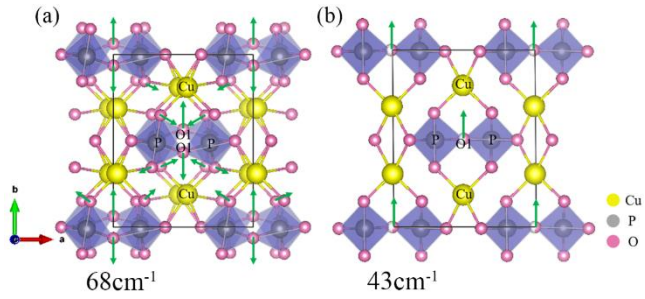

Figure 7. The schematics of (a) α-phase at the low frequency of 68 cm^{-1}, and (b) β-phase at the low frequency of 43 cm^{-1}.

Notably, compared with other NTE materials, $Cu_2P_2O_7$ has a great potential application value benefitting from its low-cost, facile synthesis and eco-friendly raw materials and product. $Cu_2P_2O_7$ oxide owns a relatively low theoretical density (4.2 g/cm^3), which is lighter than common alloys and many other NTE oxides (Table S2). The analysis of thermogravimetric-differential scanning calorimetry

(TG-DSC) proves that $Cu_2P_2O_7$ is stable and nonhygroscopic, even exposing to air for a long time (Figure S7). These superiorities impel us to explore the possible application for $Cu_2P_2O_7$. In the present study, epoxy is adopted since it possesses a strong PTE. Different ratio of $Cu_2P_2O_7$ powder were introduced to mix with epoxy. The temperature dependence of linear thermal expansion data (ΔL/L) was measured for the different weight ratio of $Cu_2P_2O_7$ to epoxy. As shown in Figure S8, one can see that the pure epoxy presents an extremely large PTE property with an average linear CTE of $\alpha_l \sim 80.79 \times 10^{-6}$ K^{-1} from 100K to 343K. The introduction of $Cu_2P_2O_7$ can effectively reduce its PTE. When the weight ratio of $Cu_2P_2O_7$ is 50%, the α_l is reduced to 52.69×10^{-6} K^{-1}. With more introduction of $Cu_2P_2O_7$, the CTE can be further reduced with α_l of 31.40×10^{-6} K^{-1} (100K ~ 343K) and 6.67×10^{-6} K^{-1} (298K – 343K) for 83%. It is worth to notice that since most engineering materials, like copper ($\alpha_l \sim 17.5 \times 10^{-6}$ K^{-1}) and aluminum ($\alpha_l \sim 23.6 \times 10^{-6}$ K^{-1}), which possess much less PTE than epoxy. Moreover, CTE and NTE temperature range of $Cu_2P_2O_7$ can be tuned by replacements of Cu or P cations, which offers wider application used in composite materials. The details are going to be published in the next paper. The present NTE oxide of $Cu_2P_2O_7$ gives a promising application in controlling of thermal expansion of common used engineering materials.

Conclusion

In summary, a strong NTE has been observed in a new oxide of $Cu_2P_2O_7$ ($\alpha_v \sim -27.69 \times 10^{-6}$ K^{-1}, 5 - 375K). The NTE mechanism has been investigated by the combined techniques of high resolution SXRD, NPD, PDF, EXAFS and DFT. The dynamically transverse motion of O atoms, especially O1 and O4 atoms, derives the coupling twist and rotation of nearly rigid PO_4 and CuO_5 polyhadra, which accounts to the large NTE in the α-$Cu_2P_2O_7$. Such large transverse vibrations of O atoms are restricted apparently in high temperature β-phase of PTE. The comprehensive NTE related good performances of the present $Cu_2P_2O_7$ possess the high promising applications.

ASSOCIATED CONTENT

Supporting Information.

Materials synthesis, Experimental methods, Data analysis procedures and Supplementary Figures. This material is available free of charge via the Internet at http://pubs.acs.org.

AUTHOR INFORMATION

Corresponding Author

* junchen@ustb.edu.cn

Notes

The authors declare no competing financial interest.

ACKNOWLEDGMENT

This work was supported by the National Natural Science Foundation of China (Grant Nos. 21825102, 21731001, and 21590793), the Fundamental Research Funds for the Central Universities, China (FRF-TP-18-001C2), the Changjiang Young Scholars Award, and the National Program for Support of Top-notch Young Professionals. Use of the Advanced Photon Source, an Office of Science User Facility operated for the U.S. Department of Energy (DOE), Office of Science, by Argonne National Laboratory, was supported by the U.S. DOE under Contract No. DE-AC02-06CH11357. We acknowledge ELETTRA Synchrotron Light Laboratory for provision of synchrotron radiation (experiment n. 20190096), as well as all the staff of XAFS Beamline for technical assistance. Variable temperature neutron powder diffraction (NPD) data was collected at the BT-1 neutron powder diffractometer at the NIST Center for Neutron Research (13K – 500K) and CSNS (China Spallation Neutron Source, GPPD, 5 – 300K). One of the authors, J. C., acknowledges the financial support of the University of Padova through the Visiting Scientist program 2019.

REFERENCES

(1) Mary, T.; Evans, J.; Vogt, T.; Sleight, A. Negative Thermal Expansion From 0.3 to 1050 Kelvin in ZrW_2O_8. *Science*. **1996**, *272*, 90.

(2) Pryde, A. K.; Hammonds, K. D.; Dove, M. T.; Heine, V.; Gale, J. D.; Warren, M. C. Rigid Unit Modes and the Negative Thermal Expansion. *Phase. Transit.* **1997**, *61*, 141.

(3) Takenaka, K.; Asano, K.; Misawa, M.; Takagi, H. Negative Thermal Expansion in Ge-free Antiperovskite Manganese Nitrides: Tin-Doping Effect. *Appl. Phys. Lett.* **2008**, *92*, 011927.

(4) Sun, Y.; Wang, C.; Wen, Y.; Chu, L.; Pan, H.; Nie, M.; Tang, M. Negative Thermal Expansion and Magnetic Transition in Anti - Perovskite Structured $Mn_3Zn_{1-x}Sn_xN$ Compounds. *J. Am. Ceram. Soc.* **2010**, *93*, 2178.

(5) Huang, R.; Liu, Y.; Fan, W.; Tan, J.; Xiao, F.; Qian, L.; Li, L. Giant Negative Thermal Expansion in $NaZn_{13}$-Type La(Fe, Si, Co)$_{13}$ Compounds. *J. Am. Chem. Soc.* **2013**, *135*, 11469.

(6) Chen, J.; Fan, L.; Ren, Y.; Pan, Z.; Deng, J.; Yu, R.; Xing, X. Unusual Transformation from Strong Negative to Positive Thermal Expansion in $PbTiO_3$– $BiFeO_3$ Perovskite. *Phys. Rev. Lett.* **2013**, *110*, 115901.

(7) Chen, J.; Hu, L.; Deng, J.; Xing, X. Negative Thermal Expansion in Functional Materials: Controllable Thermal Expansion by Chemical Modifications. *Chem. Soc. Rev.* **2015**, *44*, 3522.

(8) Li, Q.; Zhu, H.; Zheng, L.; Fan, L.; Ren, Y.; Chen, J.; Deng, J.; Xing, X. Local Structural Distortion Induced Uniaxial Negative Thermal Expansion in Nanosized Semimetal Bismuth. *Advanced Science*. **2016**, *3*, 1600108.

(9) Pachoud, E.; Cumby, J.; Lithgow, C. T.; Attfield, J. P. Charge Order and Negative Thermal Expansion in V_2OPO_4. *J. Am. Chem. Soc.* **2018**, *140*, 636.

(10) Azuma, M.; Chen, W.-t.; Seki, H.; Czapski, M.; Olga, S.; Oka, K.; Mizumaki, M.; Watanuki, T.; Ishimatsu, N.; Kawamura, N. Colossal Negative Thermal Expansion in $BiNiO_3$ Induced by Intermetallic Charge Transfer. *Nat. commun*. **2011**, *2*, 347.

(11) Azuma, M.; Oka, K.; Nabetani, K. Sci. Technol. Negative Thermal Expansion Induced by Intermetallic Charge Transfer. *Adv. Mat.* **2015**, *16*, 034904.

(12) Coates, C. S.; Goodwin, A. L. How to Quantify Isotropic Negative Thermal Expansion: Magnitude, Range, or Both? *Mater. Horiz*. **2019**, *6*, 211.

(13) Lind, C.; Wilkinson, A. P.; Hu, Z.; Short, S.; Jorgensen, J. D. Synthesis and Properties of the Negative Thermal Expansion Material Cubic $ZrMo_2O_8$. *Chem. Mater*. **1998**, *10*, 2335.

(14) Sumithra, S.; Tyagi, A.; Umarji, A. Negative Thermal Expansion in $Er_2W_3O_{12}$ and $Yb_2W_3O_{12}$ by High Temperature X-ray Diffraction. Mat. *Sci. Eng. B.* **2005**, *116*, 14.

(15) Yamamura, Y.; Horikoshi, A.; Yasuzuka, S.; Saitoh, H.; Saito, K. Negative Thermal Expansion Emerging Upon Structural Phase Transition in ZrV_2O_7 and HfV_2O_7. *Dalton. T.* **2011**, *40*, 2242.

(16) Greve, B. K.; Martin, K. L.; Lee, P. L.; Chupas, P. J.; Chapman, K. W.; Wilkinson, A. P. Pronounced Negative Thermal Expansion From a Simple Structure: Cubic ScF_3. *J. Am. Chem. Soc*. **2010**, *132*, 15496.

(17) Hu, L.; Chen, J.; Xu, J.; Wang, N.; Han, F.; Ren, Y.; Pan, Z.; Rong, Y.; Huang, R.; Deng, J. Atomic Linkage Flexibility Tuned Isotropic Negative, Zero, and Positive Thermal Expansion in $MZrF_6$ (M= Ca, Mn, Fe, Co, Ni, and Zn). *J. Am. Chem. Soc*. **2016**, *138*, 14530.

(18) Goodwin, A. L.; Kepert, C. J. Negative Thermal Expansion and Low-Frequency Modes in Cyanide-Bridged Framework Materials. *Phys. Rev. B.* **2005**, *71*, 140301.

(19) Phillips, A. E.; Goodwin, A. L.; Halder, G. J.; Southon, P. D.; Kepert, C. J. Nanoporosity and Exceptional Negative Thermal Expansion in Single-Network Cadmium Cyanide. *Angew. Chem. Int. Edit.* **2008**, *47*.1396.

(20) Duyker, S. G.; Peterson, V. K.; Kearley, G. J.; Ramirez - Cuesta, A. J.; Kepert, C. J. Negative Thermal Expansion in $LnCo(CN)_6$ (Ln= La, Pr, Sm, Ho, Lu, Y): Mechanisms and Compositional Trends. *Angew. Chem. Int. Edit*. **2013**, *52*, 5266.

(21) Chapman, K. W.; Chupas, P. J.; Kepert, C. J. Guest-Dependent Negative Thermal Expansion in Nanoporous Prussian Blue Analogues $M^{II}Pt^{IV}(CN)_6 \bullet x\ \{H2O\}(o\leq x\leq 2$; M= Zn, Cd) *J. Am. Chem. Soc.* **2005**, *127*, 17980.

(22) Gao, Q.; Chen, J.; Sun, Q.; Chang, D.; Huang, Q.; Wu, H.; Sanson, A.; Milazzo, R.; Zhu, H.; Li, Q. Switching Between Giant Positive and Negative Thermal Expansions of a $YFe(CN)_6$ - Based Prussian blue Analogue Induced by Guest Species. *Angew. Chem. Int. Edit.* **2017**, *56*, 9023.

(23) Shi, N.; Gao, Q.; Sanson, A.; Li, Q.; Fan, L.; Ren, Y.; Olivi, L.; Chen, J.; Xing, X. Negative Thermal Expansion in Cubic FeFe (CN) 6 Prussian Blue Analogues. *Dalton. T.* **2019**, *48*, 3658.

(24) Roy, R.; Agrawal, D. K.; McKinstry, H. A. Ann. *Rev.* Very Low Thermal Expansion Coefficient Materials. *Mater. Sci.* **1989**, *19*, 59.

(25) Wu, Y.; Kobayashi, A.; Halder, G. J.; Peterson, V. K.; Chapman, K. W.; Lock, N.; Southon, P. D.; Kepert, C. J. Negative Thermal Expansion in the Metal – Organic Framework Material Cu3(1,3,5 - benzenetricarboxylate)2. *Angew. Chem. Int. Edit.* **2008**, *47*, 8929.

(26) Katayama, N.; Otsuka, K.; Mitamura, M.; Yokoyama, Y.; Okamoto, Y.; Takenaka, K. Microstructural Effects on Negative Thermal Expansion Extending Over a Wide Temperature Range in β-Cu1.8Zno.2V2O7. Appl. *Phys. Lett*. **2018**, 113, 181902.

(27) Wang, H., Yang, M., Chao, M., Guo, J., Tang, X., Jiao, Y., Liang, E. Negative thermal expansion properties of $Cu_{1.5}Mg_{0.5}V_2O_7$. *Ceram. Int*. **2019**, 45, 9814.

(28) Pogorzelec-Glaser, K.; Pietraszko, A.; Hilczer, B.; Połomska, M. Structure and Phase Transitions in $Cu_2P_2O_7$. *Phase. Transit.* **2006**, *79*, 535.

(29) Evans, J.; Mary, T.; Vogt, T.; Subramanian, M.; Sleight, A. Negative Thermal Expansion in ZrW_2O_8 and HfW_2O_8. *Chem. Mater.* **1996**, *8*, 2809.

(30) Liu, Q.; Cheng, X.; Sun, X.; Yang, J.; Li, H. J. Synthesis and Characterization of Sol–gel Derived ZrV_2O_7 Fibers with Negative Thermal Expansion Property. *Sol-Gel. Sci. Techn.* **2014**, *72*, 502.

(31) Wang, X.; Huang, Q.; Deng, J.; Yu, R.; Chen, J.; Xing, X. Phase Transformation and Negative Thermal Expansion in Ta-VO_5. *Inorg. Chem.* **2011**, *50*, 2685.

(32) Evans, J.; Mary, T.; Sleight, A. Negative Thermal Expansion in $Sc_2(WO_4)_3$. *J. Solid State Chem.* **1998**, *137*, 148.

(33) Chatterji, T.; Henry, P. F.; Mittal, R.; Chaplot, S. Negative thermal expansion of ReO_3: Neutron Diffraction Experiments and Dynamical Lattice Calculations. *Phys. Rev. B.* **2008**, *78*, 134105.

(34) Amos, T.; Sleight, A. Negative Thermal Expansion in Orthorhombic $NbOPO_4$. *J. Solid State Chem*. **2001**, *160*, 230.

(35) Krasnenko, T.; Zolotukhina, L.; Andrianova, L. Thermal Strain in Zinc Pyrovanadate. *Inorg. Mater.* **2000**, *36*, 1032.

(36) Zhang, N.; Li, L.; Wu, M.; Li, Y.; Feng, D.; Liu, C.; Mao, Y.; Guo, J.; Chao, M.; Liang, E. Negative Thermal Expansion and Electrical Properties of α-$Cu_2V_2O_7$. *J. Eur. Ceram. Soc.* **2016**, *36*, 2761.

(37) Forster, P.; Yokochi, A.; Sleight, A. Enhanced Negative Thermal Expansion in $Lu_2W_3O_{12}$. *J. Solid. State. Chem.* **1998**, 157.

(38) Forster, P.; Sleight, A. Int. J. Negative Thermal Expansion in $Y_2W_3O_{12}$. *Inorg. Mater*. **1999**, *1*, 123.

(39) Fornasini, P.; Ahmed, S. I.; Sanson, A.; Vaccari, M. EXAFS Studies of Negative Thermal Expansion Materials. *Physica. Status. Solidi. B* **2008**, *245*, 2497.

(40) Sanson, A. *J.* On the Einstein Model for EXAFS Parallel and Perpendicular Mean-Square Relative Displacements. *Synchrotron. Radiat*. **2008**, 15, 514.